JOURNAL OF GEOPHYSICAL RESEARCH, VOL. 88, NO. A6, PAGES 4793–4804, JUNE 1, 1983

Magnetic Field Line Reconnection Experiments 5. Current Disruptions and Double Layers

R. L. STENZEL, W. GEKELMAN, AND N. WILD

Department of Physics, University of California, Los Angeles, California 90024

In a large laboratory plasma a current sheet is generated in the process of magnetic field line reconnection. The stability of the sheet with respect to local current increases is investigated. When the current density in the center of the sheet exceeds a critical value, spontaneous local current disruptions are observed. The current from the center of the sheet moves out to the sides. Magnetic flux variations in regions remote from the current sheet generate an inductive voltage in the current loop that drops off inside the plasma in the form of a potential double layer. This leads to particle acceleration with velocities much larger than those expected from the steady state electric fields in the plasma. The particle beams acquire their energy at the expense of the stored magnetic field energy of the current system. Beam-plasma instabilities are generated that dissipate some of the directed kinetic energy and heat the background plasma. A model for the mechanism of the current disruptions is formulated. The potential structure leads to ion expulsion creating a localized density drop. The associated current drop in an inductive circuit drives the potential structure, thereby providing feedback for the disruptive instability. It saturates at a total current loss upon which the current system recovers, and the process repeats randomly. Similarities and differences to magnetospheric substorm phenomena are pointed out.

INTRODUCTION

The stability of current systems in space plasmas continues to be of great interest. Impulsive phenomena such as solar flares and magnetic substorms are frequently interpreted in terms of current disruptions [*Alfvén*, 1977; *Akasofu*, 1977; *Syrovatskii*, 1981; *Spicer*, 1982]. The flux changes associated with modifications of a current system lead to inductive electric fields and particle accelerations [*Heikkila and Pellinen*, 1977]. It is important to consider the properties of the entire current system in order to understand the coupled electromagnetic processes and the plasma dynamics. For example, when the current system involves the formation of a double layer, the evolution of this localized structure depends on the distant circuit properties such as distributed inductances, resistances, and energy sources [*Smith*, 1982]. Detailed observations of magnetospheric current systems are very difficult to perform [*Roederer*, 1979; *Potemra*, 1979; *Stern*, 1977], calling for computer simulations [*Dawson*, 1981; *Hayashi and Sato*, 1978; *Leboeuf et al.*, 1982] and laboratory models [*Podgorny et al.*, 1980; *Baum and Bratenahl*, 1982; *Stenzel et al.*, 1982*a*] to provide additional insight.

Current systems with magnetic null points have been studied in the laboratory for many years [*Frank*, 1976; *Ohyabu et al.*, 1974; *Baum and Bratenahl*, 1980*a*; *Stenzel et al.*, 1982*b*]. In many of these experiments it is observed that a phase of steady current flow is followed by a disruption of the plasma current in the neutral sheet. The plasma is ejected and lost, which terminates the experiment. The mechanisms leading to such disruptions are not well understood. Anomalous resistivity [*Baum and Bratenahl*, 1980*a*], double layers [*Baum and Bratenahl*, 1980*b*], and tearing modes [*Bulanov and Syrovatskii*, 1976] have been proposed but not confirmed owing to diagnostic difficulties with high density ($n_e \simeq 10^{15}$ cm^{-3}), pulsed ($t \simeq$ 1-10 μs), small ($\sim$1 cm $\times$ 5 cm) plasmas. Since detailed diagnostics is a major motivation for performing modeling experiments, we have designed and operate a reconnection experiment at lower densities ($\lesssim 10^{12}$ cm^{-3}), larger scale lengths ($\sim$30 cm $\times$ 80 cm $\times$ 200 cm), and longer pulse durations (200 μs). With the help of a digital data acquisition system we have studied the space time evolution of the magnetic fields [*Stenzel and Gekelman*, 1981*a*], the plasma parameters [*Gekelman and Stenzel*, 1981], the fluid dynamics [*Gekelman et al.*, 1982], and the energy flow [*Stenzel et al.*, 1982*b*]. In the present paper, we continue the sequence by presenting detailed observations of current disruptions with double layer formation reported briefly in a recent Letter [*Stenzel et al.*, 1982*a*].

Spontaneous current disruptions are observed in the center of a neutral sheet when the local current density exceeds a critical value. The disruptions are localized, i.e., the current is diverted to the sides of the neutral sheet. The associated flux changes produce an inductive voltage in the circuit that drops off at the locations of the current disruption, i.e., inside the plasma, in a thin layer ($d \simeq 100\ \lambda_D$). At this double layer, particle beams are generated with energies corresponding to the inductive voltage that far exceeds the dc circuit voltage. Thus, at the double layer the conversion of magnetic to kinetic energy takes place. It is interesting to note that most of the available magnetic energy is stored remotely in the external circuit rather than locally in the neutral sheet. Similar situations may also arise in space as discussed by *Spicer* [1982]. The rapid ejection of particles at the double layer lowers the local plasma density, hence current density that drives the disruptive instability.

The observed current disruptions and double layers involve coupled electric and magnetic phenomena. They are three dimensional and nonstationary. They depend on the magnetic field topology: disruptions are seen for a neutral sheet but not for a magnetic island. Hence, they differ in many respects from the current fluctuations associated with purely electrostatic double layers [*Iizuka et al.*, 1982] but have some similarity to current chopping of arc plasmas [*Tuma and Ware*, 1968; *Torvén and Babić*, 1975].

EXPERIMENTAL ARRANGEMENT

The reconnection experiments are performed in a cylindrical vacuum chamber (1.5 m diameter, 2 m length) in which a low

Paper number 3A0428.
0148-0227/83/003A-0428$05.00

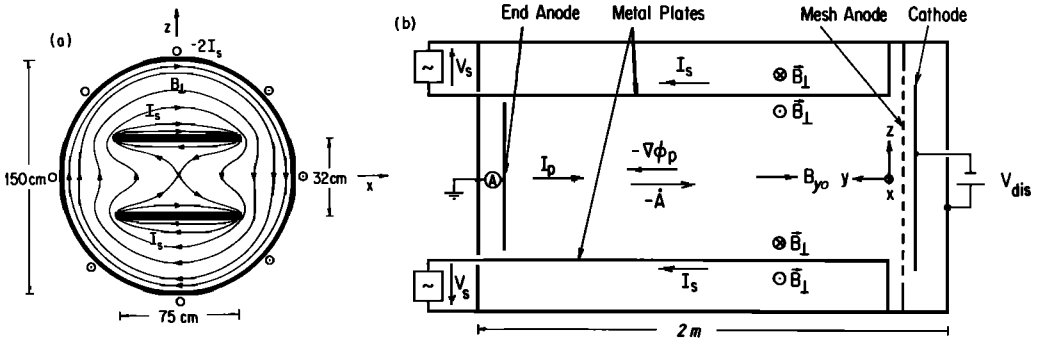

Fig. 1. Schematic view of the experimental setup. (*a*) Cross section of the cylindrical chamber showing the two flat plates with pulsed axial currents I_s that return on the chamber wall. Typical magnetic field lines in vacuum indicate the presence of an X point on axis. (*b*) Side view of the device with characteristic fields and currents. Note the presence of a dc axial magnetic field component B_{y0} in addition to the transverse fields $\mathbf{B}_{\perp(t)}$. The discharge plasma is produced with the 1 m diameter hot cathode at the right, the plasma current I_p flows to the end anode at the left, which is modified as shown in Figure 2.

pressure ($p \lesssim 10^{-4}$ torr, A, H_2) discharge is produced with a one meter diameter oxide-coated cathode (Fig. 1). The emission properties of this special cathode provide a high quality laboratory plasma of the following properties: Uniformity over large scale lengths ($\Delta n/n \simeq 10\%$ over 80 cm across $\mathbf{B}_0$, 180 cm along $\mathbf{B}_0$), nearly collisionless, high beta parameters (density $n_e \lesssim 10^{12}$ cm^{-3}, temperature $kT_e \simeq 10$ eV, electron-ion mean free path $l_{ei} \simeq 200$ cm, axial magnetic field $B_0 \simeq 12$ G, $\beta = nkT/(B^2/2\mu_0) \simeq 2$], high repetition rate ($t_{rep} \simeq 2$ s), and good reproducibility ($\delta n/n \lesssim 5\%$) of the pulsed discharge ($V_{dis} \simeq 40$ V, $I_{dis} \simeq 1500$ A, $t_{dis} \simeq 5$ ms). The discharge pulse length is more than sufficient to reach steady-state plasma conditions, at which time the reconnection experiment is initiated. This involves establishing a transverse magnetic field $\mathbf{B}_\perp = (B_x, B_z)$ with null point. Note that we have adopted x, y, z coordinates commonly used for the magnetotail where the y direction is along the separator, x is along the neutral sheet, and z is normal to it. A large sinusoidal current pulse ($I_s \simeq 20$ kA, rise time $t_r \simeq 100$ μs) is drawn axially through two parallel aluminum plates (75 cm wide, 33 cm spacing, 180 cm length) located on top and bottom of the plasma column. The plates are insulated from the plasma that is confined to the space between them. Axial and average transverse magnetic fields are of comparable strength.

The transverse magnetic field geometry in vacuum is shown schematically in the cross sectional view of the device (Figure 1*a*). Without plasma there is an X type neutral point on the axis of the device. However, with plasma, axial plasma currents are induced ($I_p \gtrsim 1000$ A) that modify the magnetic field topology. The self-consistent current distribution and field topology can result in the formation of a classical neutral sheet [*Dungey*, 1958]. The plasma current driven by inductive and space charge electric fields ($\mathbf{E} = -\dot{\mathbf{A}} - \nabla\phi_p$) is mainly carried by the electrons. During the initial phase of external current rise ($dI_s/dt > 0$, $0 < t \lesssim 100$ μs) the electrons drift from the cathode toward the end anode. The current closes via the grounded chamber walls to the cathode. No net current flows to the insulated plates or the radial chamber walls which are well separated from the plasma column.

The cathode emits as many electrons as are collected at the end plate so as to maintain approximate space charge neutrality. However, as the applied inductive electric field ($\dot{A} \lesssim 0.5$ V/cm) can exceed the classical runaway field [*Dreicer*, 1959] ($E_r \simeq m_e \nu_{ei} v_e/e \simeq 0.1$ V/cm, where $v_e^2 = 2kT_e/m_e$) and the space charge limited emission [*Langmuir*, 1929] does not provide for current densities $j \gtrsim nev_e$ the plasma sets up an axial space charge electric field $-\nabla\phi_p$ opposite to the induced field. This shielding effect limits the electron drift to $v_d < v_e$, at least on the average over the entire plasma cross section. Lack of additional ionization due to burn out of neutrals [*Gekelman and Stenzel*, 1981] limits the average current density. Locally, however, the current density can be enhanced at the expense of the surrounding values. Of particular interest is the stability of a current sheet when the current density at its center is steadily increased. This situation seems to occur in the build-up phase of a magnetic substorm in the magnetotail [*McPherron*, 1979].

In order to control the local current density in the neutral sheet the end anode is modified. As shown schematically in Figure 2 the central section (6 cm × 13 cm) of the large grounded end anode (32 cm × 75 cm) is separated and connected to an external dc supply. When the positive supply voltage V_{adc} is increased, the current I_a to the center plate rises while the large end plate current decreases. In order to avoid generating gradients during the plasma production the small anode is grounded via a diode until the reconnection experiment begins, at which time the dc supply is switched on via a silicon controlled rectifier.

Both external measurements of currents and voltages are performed as well as internal diagnostics of plasma and field properties. Space and time resolved data on density temperature, particle distributions, potentials, magnetic fields, and instabilities are obtained from Langmuir probes, magnetic loops, rf probes, and a novel directional energy analyzer [*Stenzel et al.*, 1983]. A digital data acquisition system consisting of

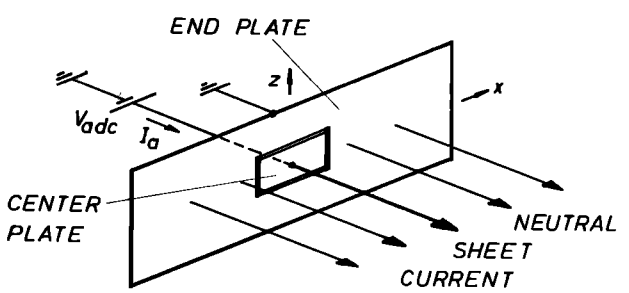

Fig. 2. End anode modified for the disruption experiments. Central section (6 cm × 13 cm) can be biased positively with respect to the grounded large (32 cm × 75 cm) end plate. With this arrangement the current density in the neutral sheet center can be raised until limited by disruptive instabilities.

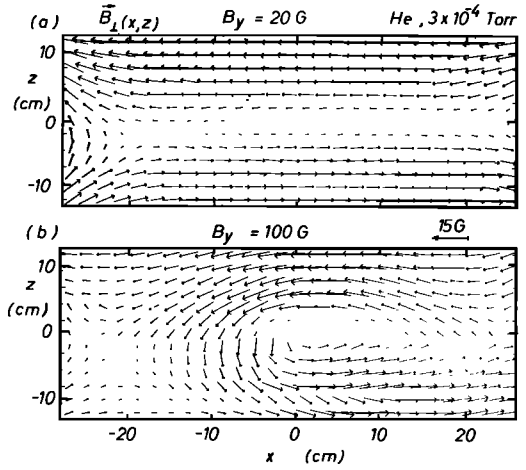

Fig. 3. Typical transverse magnetic field topologies $\mathbf{B}_\perp(x, y)$ in the reconnection experiment. (*a*) Neutral sheet. (*b*) Magnetic island.

fast analog-to-digital converters, minicomputer, array processor, and data link to a large off-site computer is used for processing field and distribution function measurements.

Experimental Results

Before describing the observations of current disruptions, it is helpful to show the basic magnetic field topology of the experiment. Figure 3 shows measured vector fields of the transverse field components $\mathbf{B}_\perp = (B_x, B_z)$ in the transverse x-z plane ($y = 137$ cm) at a fixed time $t \simeq 30$ μs during the external current rise. The data are obtained from repeated experiments and represent ensemble averages over ten shots at each of the 350 positions. Fluctuations around the mean values are the subject of a separate investigation [*Gekelman et al.*, 1983]. Figure 3*a* shows the classical neutral sheet topology. It is associated with a current sheet $J_y = (\nabla \times \mathbf{B}_\perp)_y/\mu_0$ flowing axially along the uniform B_y field. This is the characteristic field topology in the parameter regime of the present experiment. However, it is not the only self-consistent configuration of field and current distributions. Figure 3*b* depicts a condition where the plasma current is concentrated near the center of the column rather than in an elongated sheet. The magnetic field topology is that of a magnetic island with an adjacent X point at each side. This field configuration can arise through tearing of the neutral sheet [*Furth et al.*, 1963]. It is readily observed in the presence of a strong axial field component B_y that, however, is not employed in the current disruption experiments. Island formation may also occur when the current profile is controlled by a special configuration of the end anode, as is the case in the experiments described below.

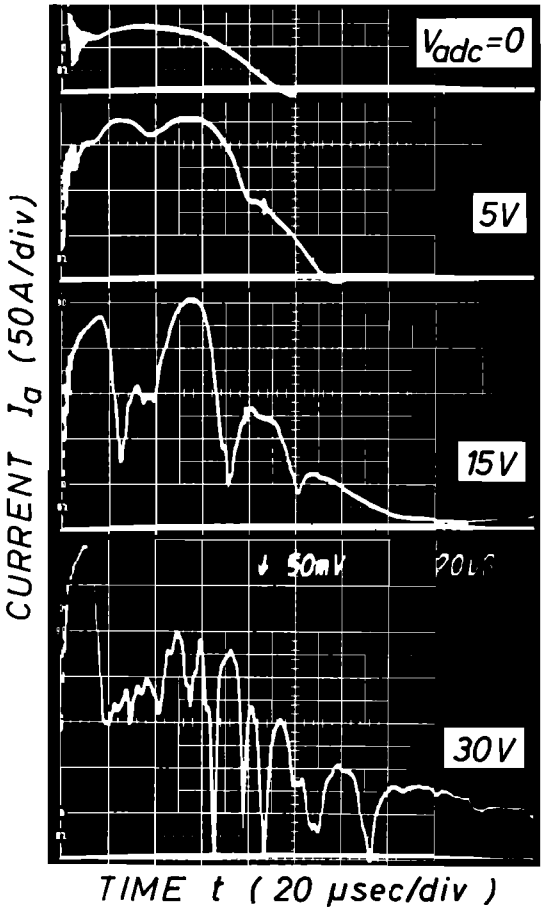

Fig. 4. Current $I_{a(t)}$ to the center end plate at different dc supply voltages V_{adc}. With increasing currents, spontaneous disruptions develop that can lead to a total current loss.

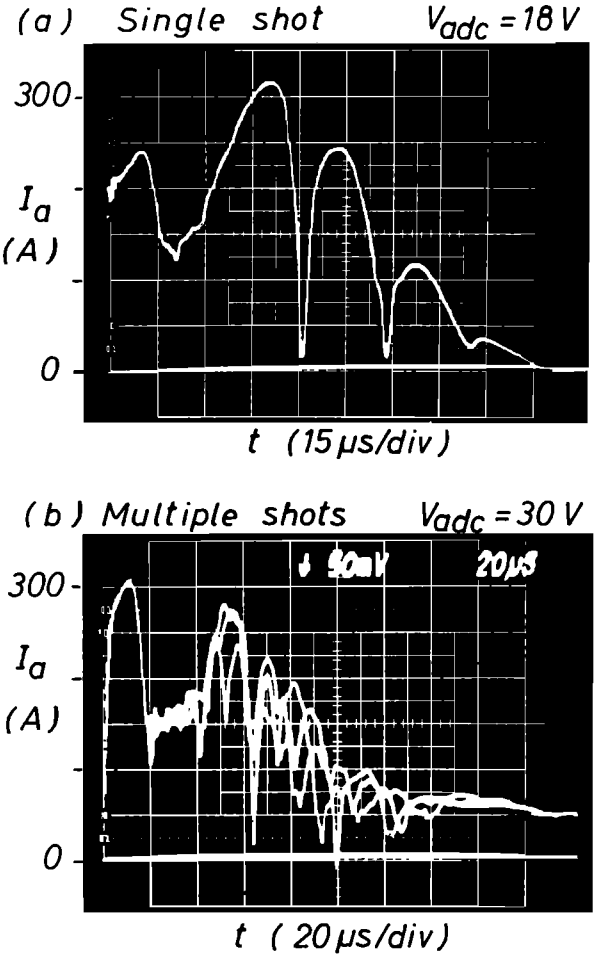

Fig. 5. Comparison of the unstable end plate current $I_{a(t)}$ for (*a*) one and (*b*) several repeated experiments, indicating the randomness in amplitude and timing of the disruptions.

Current Disruptions

We first describe the current voltage characteristics of the neutral sheet system perturbed by the biased small end plate.

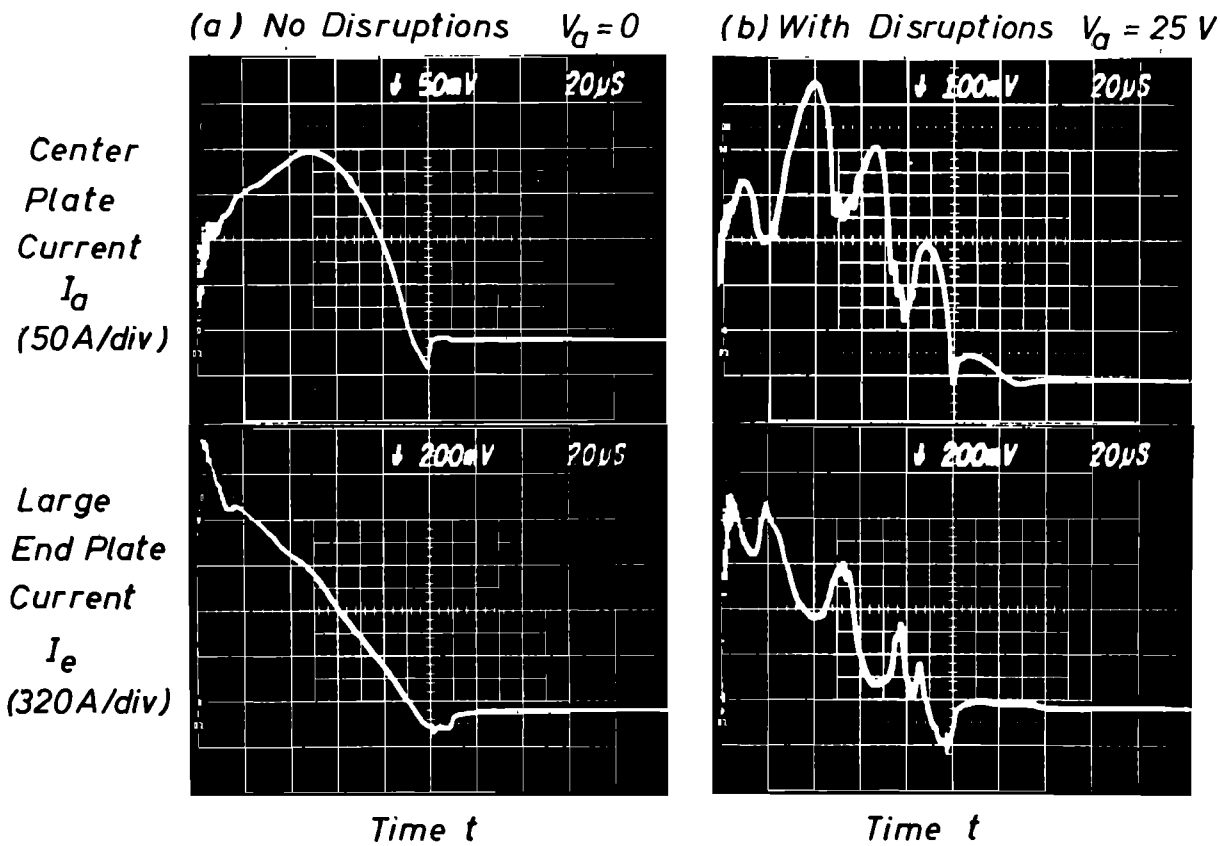

Fig. 6. Currents to the small and large end plates (*a*) in the absence of disruptions and (*b*) with disruptions. Note change in scale for I_a to 100 A/div in Figure 6*b*. Comparison of the unstable currents shows that a current drop in I_a results in a corresponding increase of I_e such that the total plasma current is nearly constant.

Figure 4 shows single shot traces of the end plate current I_a versus time at different applied dc potentials V_{adc}. For $V_{adc} = 0$ the entire end anode system (Figure 2) is an equipotential surface. The currents to the large and small end plate have similar waveforms and differ only in magnitude owing to the different collecting areas. The sinusoidal current waveform is the response to the applied inductive electric field $E_i \propto \cos \omega t$ for $0 < t < \pi/2\omega \simeq 100$ μs. When the electric field changes sign ($100 \lesssim t \lesssim 200$ μs) the plasma current reverses and flows to the gridded anode adjacent to the cathode (Figure 1*b*). The plasma potential near the end anode becomes highly positive such that no end anode current can flow. Potential profiles have been shown earlier in Figure 8 of paper 2 [*Gekelman and Stenzel*, 1981].

When, by raising the bias voltage V_{adc} the small end plate current I_a is increased, the smooth current waveform develops repeated drops. With increasing peak currents the perturbations become more frequent, shorter in duration and larger in amplitude, eventually approaching total current disruptions.

The random nature of the current disruptions is demonstrated in Figure 5. While a single shot trace such as shown in Figure 5*a* may give the impression of a clearly periodic disruption process, the superposition of three traces in Figure 5*b* indicates a rather random behavior in timing and amplitude of the spontaneously occurring disruptions. Only the first current drop is reproducible, reflecting the high shot-to-shot reproducibility of the initial plasma parameters.

The disruption of a few hundred amperes of current to the center plate does not, surprisingly, affect the cathode current. Thus the disruption involves a current redistribution rather than a net current loss. The only alternate path for the perturbed current is to flow to the large grounded end plate. Figure 6 shows current waveforms for both the small and the large end anode. For $V_{adc} = 0$ there are no disruptions (Figure 6*a*), but with positive bias both the center plate current and the large end plate current exhibit current pulses. These are of the same magnitude (note a scale change to 100 A/div. for I_a in Figure 6*b*), but of opposite phase, i.e., the current lost by the small anode is gained by the large anode. Thus, the sum of both currents that make up the total induced plasma current remains essentially constant. The current must branch somewhere in the plasma during the disruption. By in situ measurements the location and mechanism of the current disruption will be established.

Before describing the results of the plasma diagnostics, we point out another property of the current flow. When the large end anode is disconnected from ground, the plasma current can flow only to the small end anode. Analogous to Figure 4 we show in Figure 7 the current waveforms $I_{a(t)}$ at different dc potentials V_{adc}. There are no current disruptions observed even for peak currents $I_{amax} \simeq 600$ A, exceeding twice the value at which previously total disruptions occurred. With the current concentrated near the axis the magnetic field topology is that of a magnetic island similar to Figure 3*b*. This configuration is stable, in contrast to the neutral sheet topology (Figure 3*a*).

Plasma Potential

A small plane Langmuir probe has been placed radially into the plasma near the end anode. Inserted through bellows the probe can be moved in all three dimensions so as to provide

space-time information of the plasma potential, density, and temperature.

Starting at the small end anode we observe its potential with respect to ground during current disruptions. Figure 8 shows both waveforms, current $I_{a(t)}$, and voltage $V_{a(t)}$, from two similar shots. At every current disruption the anode voltage exhibits a sharp peak that can exceed the applied dc potential by a factor of 5 to 10. These voltage spikes are caused by inductive effects that modify the instantaneous plate voltage to become $V_{a(t)} = V_{adc} - LdI_{a(t)}/dt$. The inductance L in our experiment is not a lumped circuit element but represents the distributed inductance of the current path between the plate and ground. It is inherent to any extended current system. From the data we estimate its value to be $L = V_i \Delta t/\Delta I \simeq 50\text{V}\ 5\mu\text{s}/250\text{A} = 1\ \mu\text{H}$, which is a realistic value for the geometry of our circuit and the internal inductances of the high current switch and capacitor bank inside the dc supply.

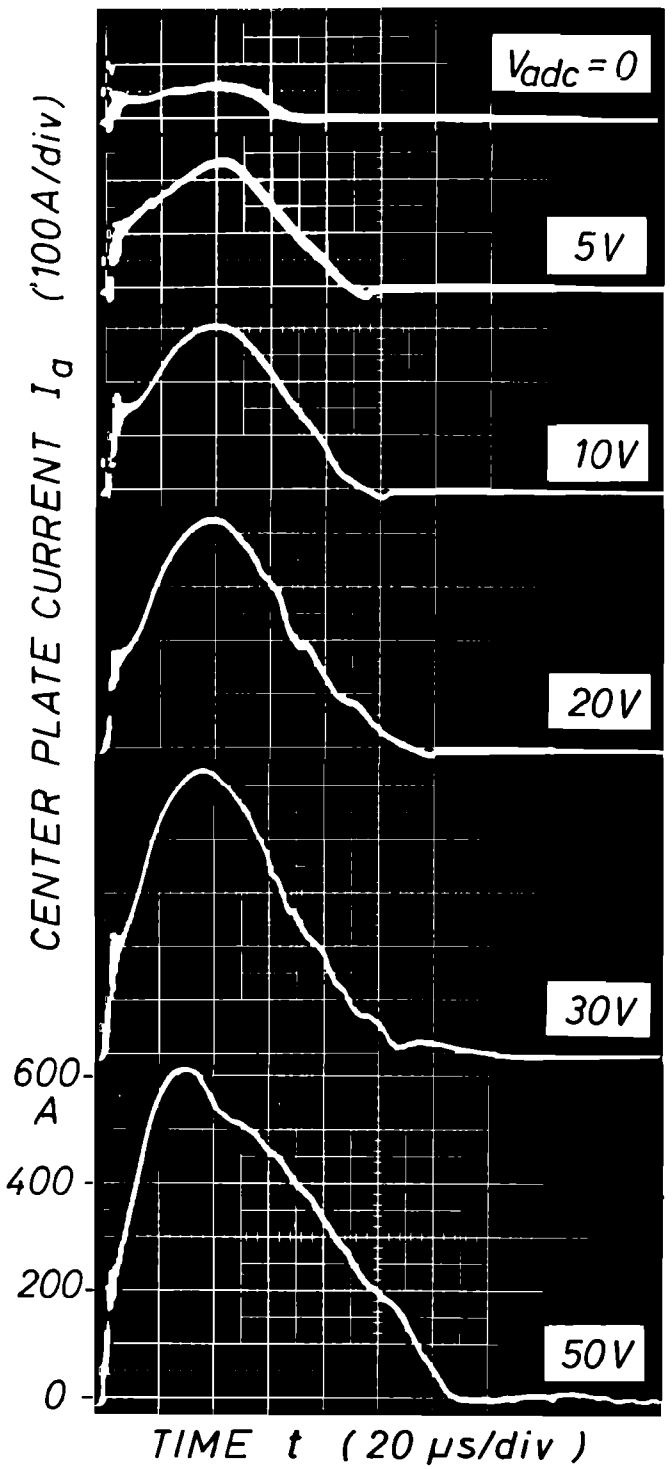

Fig. 7. Small end plate currents $I_{a(t)}$ at different supply voltages V_{adc}. In contrast to Figure 4 the large end plate is floating ($I_e = 0$) so that the entire plasma current flows to the center plate, resulting in a magnetic island topology. No current disruptions are observed.

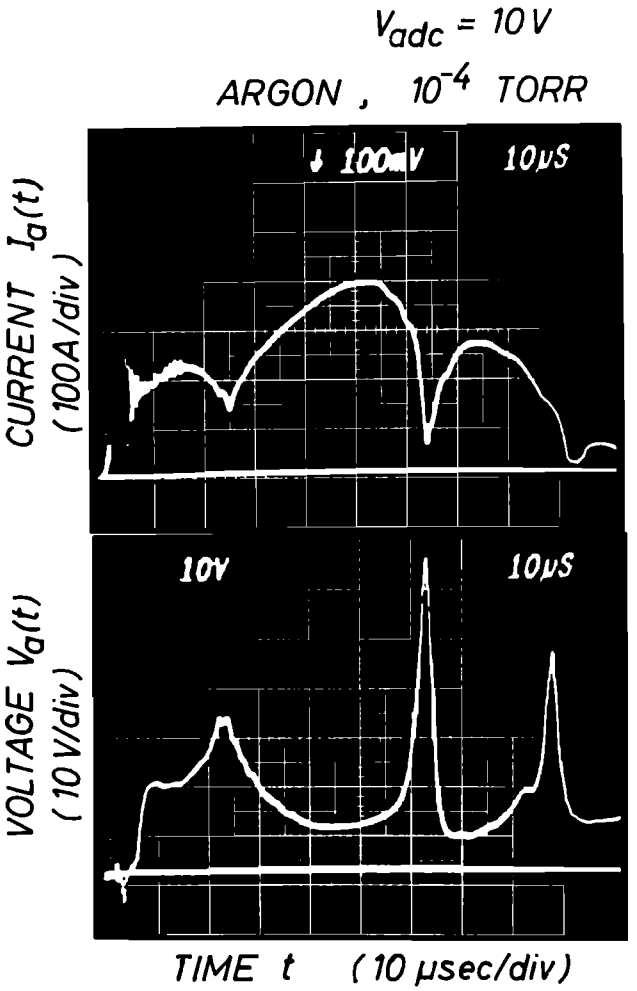

Fig. 8. Disrupted center plate current $I_{a(t)}$ (top trace) and instantaneous plate voltage $V_{a(t)}$ (bottom trace) measured in situ. At each disruption a voltage spike is generated owing to the distributed circuit inductance L. Note that $LdI_a/dt \gg V_{adc} = 10\text{V}$.

It is an important question how the large positive anode potential joins to the normally much lower plasma potential. Figure 9 describes the temporal behavior of the plasma potential at a position $\Delta y \simeq 5$ cm on axis in front of the small end anode. Owing to its good reproducibility we concentrate on the first disruption, although it is only a partial disruption ($\Delta I_a/I_a \simeq 50\%$). The top trace of Figure 9*a* shows the current waveform $I_{a(t)}$, and below it the timing of three rapidly swept Langmuir probe traces $I_{p(t)}$, one before the first disruption ($t_1 \simeq 15\ \mu$s), the second during the current minimum ($t_2 \simeq 25\ \mu$s), and the last one after the disruption ($t_3 \simeq 35\ \mu$s). Expanded views of the probe traces are shown in Figure 9*b*, together with the probe voltage ramp $V_{p(t)}$ on the top trace. The plasma potential, identified by arrows at the knee of the Langmuir

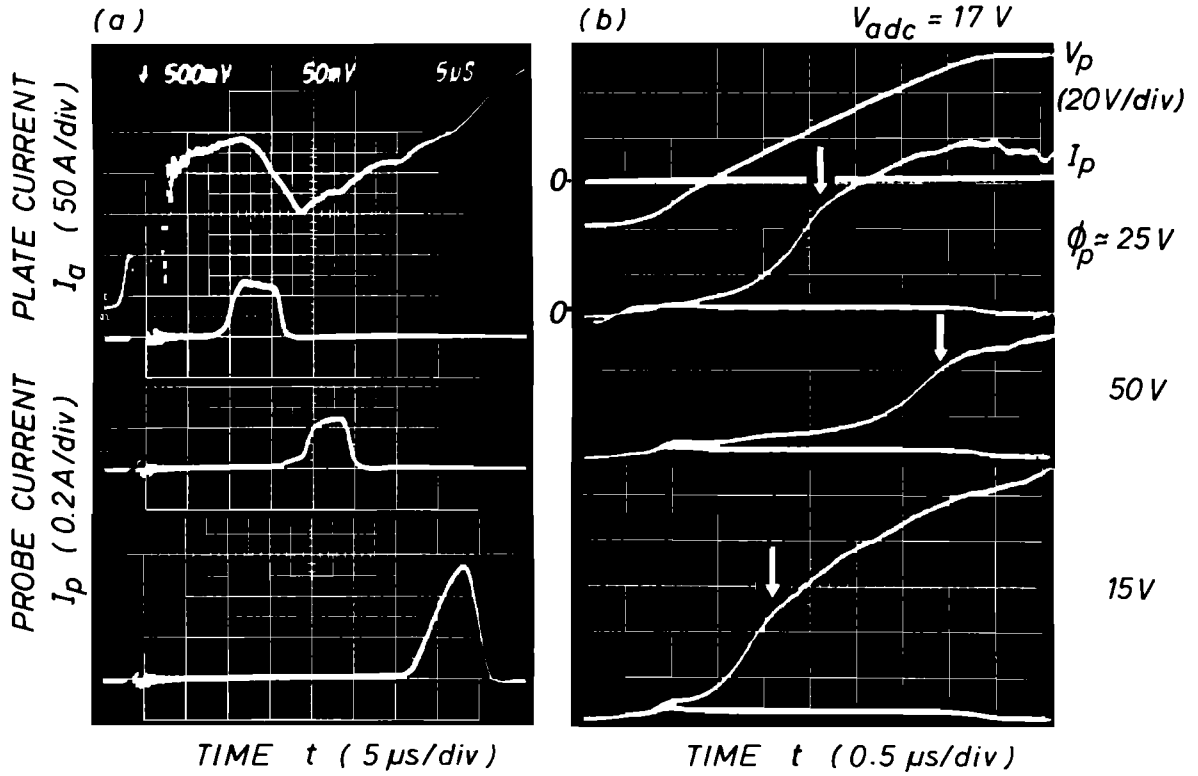

Fig. 9. Temporal variations of the plasma potential during current disruptions as derived from rapidly swept Langmuir probe traces. (*a*) Center plate current (top trace) with first disruption at $t \simeq 25$ μs and three probe traces taken before, during, and after the disruption. (*b*) Expanded view of the three probe currents together with the probe voltage ramp (top trace). The plasma potential ϕ_p indicated by arrows shows a large increase during the disruption. ($\Delta y \simeq 5$ cm).

probe characteristics, shows a dramatic increase during the current disruption to $\phi_p \simeq 50$ V. The local plasma potential increases together with the plate potential such that the inductive voltage does not drop off in an anode sheath but somewhere well within the plasma. It is also interesting to note that during the disruption the electrons exhibit a large energy spread ($\Delta E \simeq 50$ eV) with high-energy particles, forming a non-Maxwellian tail. Velocity distribution functions will be presented further below.

The spatial distribution of the plasma potential has been mapped during the current disruption. Figure 10 shows the axial dependence $\phi_{p(y)}$ in the direction of **B**. Again, the plasma potential is derived from Langmuir probe traces $I_p(V_p)$ (Figure 10*a*) swept out rapidly during the current minimum. Multiple shot traces are shown to indicate the reproducibility and accuracy of the potential measurements. The potential is found to drop off rapidly in a highly localized region at $\Delta y \simeq 6$ cm from the end anode (Figure 10*b*). The width of the potential step is approximately $d \simeq 5$ mm $\simeq 100\ \lambda_D$, resulting in a localized electric field $\Delta\phi/d \simeq 60$ V/cm. The transition has the characteristic properties of a potential double layer [*Block*, 1978; *Schamel*, 1982; *Torvén*, 1979; *Quon and Wong*, 1976; *Stenzel et al.*, 1981]; however, it is non-stationary, three dimensional, and embedded in a nonuniform magnetic field. The strong fluctuations in the probe traces at the double layer (Figure 10*a*, middle trace) are due to fluctuations in the position of the

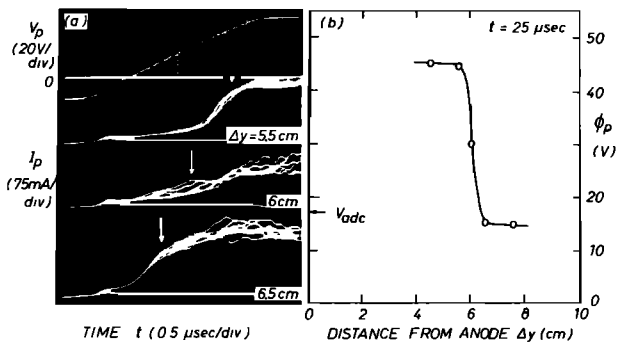

Fig. 10. Spatial variation of the plasma potential during a current disruption ($t \simeq 25$ μs). (*a*) Langmuir probe voltage V_p (top trace) and currents I_p at three different axial distances Δy from the end anode. Multiple traces show repeatability and fluctuations. (*b*) The plasma potential $\phi_{p(\Delta y)}$ indicated by arrows in (*a*) drops off axially in a narrow region ($d \simeq 5$ mm $\simeq 100\ \lambda_D$), forming a potential double layer. The inductive circuit voltage rather than the dc voltage determines the double layer potential ($\Delta\phi_p \simeq LdI/dt$).

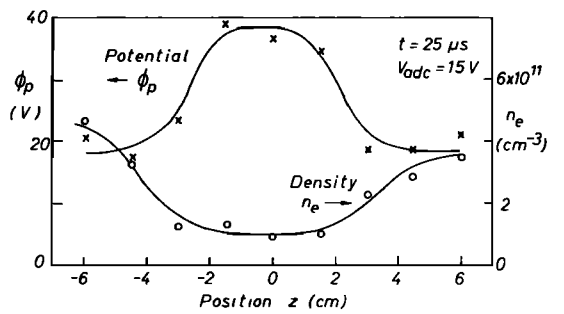

Fig. 11. Spatial variation of plasma potenial $\phi_{p(z)}$ and electron density $n_{e(z)}$ in the transverse direction across the perturbed current channel ($x \simeq 0$, $\Delta y \simeq 4$ cm). The density loss caused by ion expulsion from the positive potential region is thought to be responsible for the current drop.

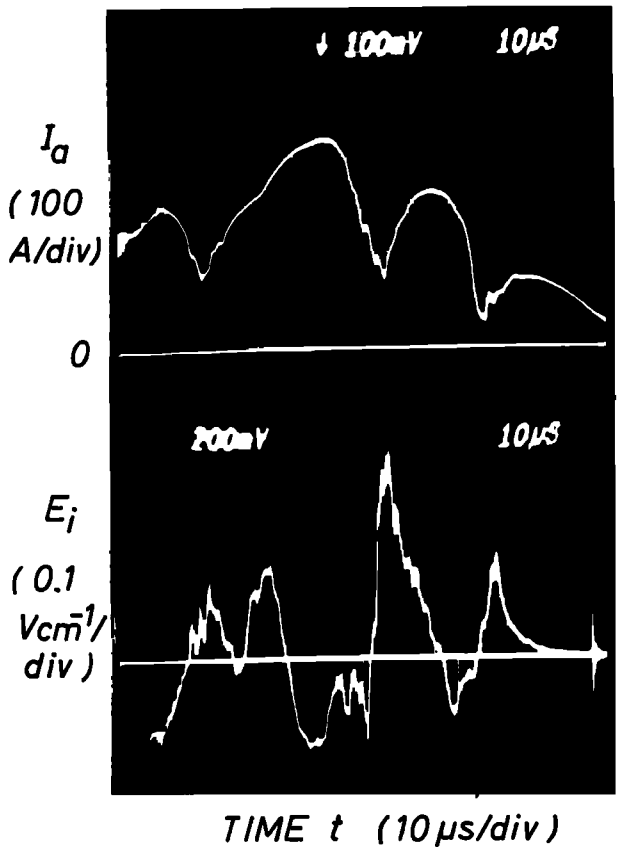

Fig. 12. Center plate current $I_{a(t)}$ (top trace) and inductive electric field $E_i = -\partial A_y/\partial t$ inside the plasma ($x = z = 0$, $\Delta y \simeq 4$ cm). The latter is obtained from a large magnetic loop (3 cm × 25 cm) measuring the time rate of change of the perturbed transverse flux per axial length, $d\psi/dy = \dot{A}_y$.

double layer. At the low potential side ($\Delta y > 6$ cm), significant low-frequency (0.2–2 MHz) density fluctuations are visible, and at the high-potential side, tails in the electron distribution are apparent.

In the transverse direction the potential distribution $\phi_p(z)$ at $\Delta y \simeq 5$ cm, $x = 0$ is as shown in Figure 11. The large positive plasma potential extends over a region slightly smaller than the height of the small anode ($\Delta z = 6$ cm). Similarly, in x direction the potential hill has a width approaching the plate width ($\Delta x = 13$ cm). The Langmuir probe traces have also been analyzed to obtain the electron density. As shown in Figure 11 a strong density depression is found in the high potential region. The density loss is due to transverse and axial potential gradients $-\nabla\phi_p$ that accelerate the essentially unmagnetized ions away from the high-potential region. The density loss associated with the ion expulsion is the main reason for the current loss to the end anode.

It is interesting to note that the potential drop is localized in a single strong double layer rather than in a series of weak double layers ($e\phi/kT \simeq 1$). The latter should be possible since the conditions for ion acoustic double layers [*Sato and Okuda*, 1981] are readily satisfied, i.e., $T_e \gg T_i$ and the system length ($L \simeq 2$ m) is very large compared with the Debye length ($L/\lambda_D \simeq 40{,}000$).

While the present discussion has been concentrated on the electrostatic fields associated with plasma potential gradients ($\mathbf{E}_e = -\nabla\phi_p$) there are also inductive electric fields inside the plasma, $\mathbf{E}_i = -\partial\mathbf{A}/\partial t$, where $\mathbf{A}$ is the vector potential ($\nabla \times \mathbf{A} = \mathbf{B}$). These can be measured with a long rectangular loop probe which links the magnetic flux ψ in the x-y plane [*Stenzel et al.*, 1982*b*]. The short wire section ($\Delta y \simeq 3$ cm) is placed along the axis, the long parallel wires are leading out in the x direction. The open loop voltage V_i yields the predominantly axial inductive electric field, $-\dot{A}_y = -\dot{\psi}/\Delta y = V_i/\Delta y$. Figure 12 shows the waveforms of the disrupted current (Figure 12*a*) and the inductive electric field $-\dot{A}_y$ in the perturbed current channel ($\Delta y \simeq 4$ cm). One can see enhanced electric fields during disruptions that are directed so as to accelerate electrons toward the plate and ions away from it.

Although much smaller than the highly localized electrostatic field of the double layer, the inductive electric field contributes owing to its larger spatial extent to the particle energization. With increasing distance from the current disruption region the magnetic perturbations decrease, disperse, and assume a turbulent character to be discussed further below. A detailed study of the three-dimensional time varying magnetic field topology in the disruption region has not yet been performed.

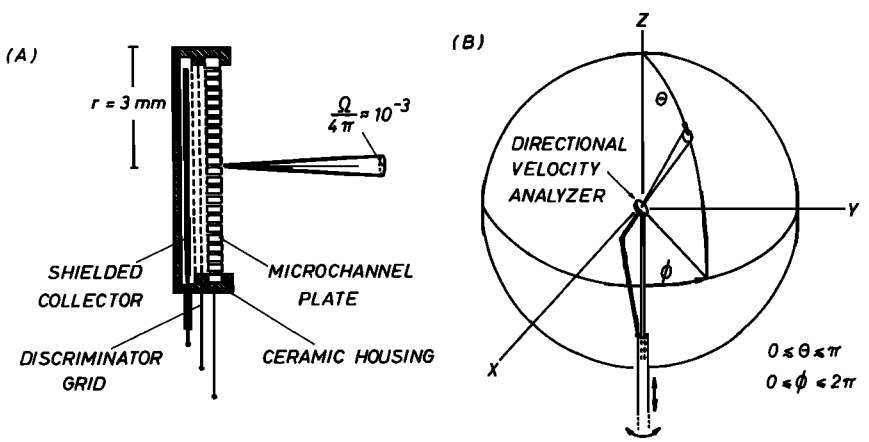

Fig. 13. (*a*) Schematic view of the directional velocity analyzer. The microchannel plate provides for angular resolution, while the retarding potential analyzer measures the speed distribution. (*b*) Probe mounting of the velocity analyzer provides for angular rotation in θ and ϕ so as to cover velocity space, as well as translational motions for resolving real space. Fast temporal sweeps yield fully resolved distribution functions, $f(\mathbf{v}, \mathbf{r}, t)$.

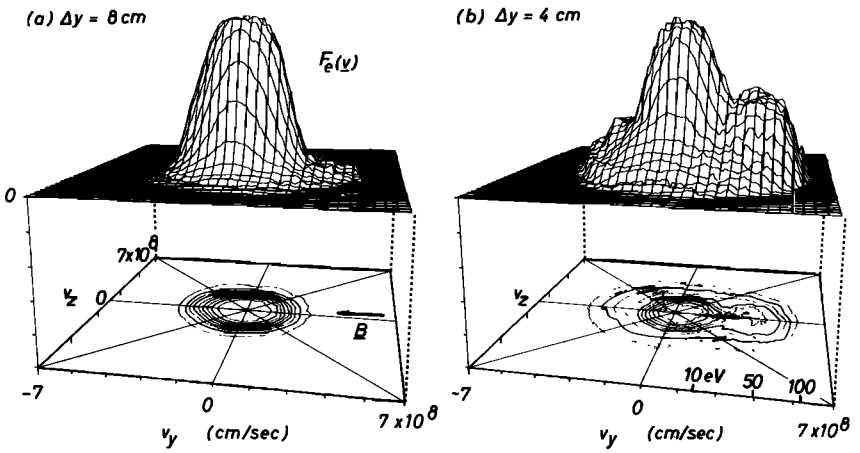

Fig. 14. Electron distribution functions during current disruptions (*a*) at the low potential side and (*b*) the high potential side of the double layer. The population of free electrons accelerated to energies $\frac{1}{2}mv_y^2 \simeq e\Delta\phi_p \simeq 35$ eV is clearly visible.

Particle Distributions

Formation of double layers in collisionless plasmas generally involves non-Maxwellian velocity distribution functions. Since transport processes and instabilities strongly depend on the shape of the distribution function, its measurement is important for the understanding of current disruptions and impulsive reconnection events.

In order to measure anisotropic velocity distribution functions with a particle detector, it has to have directional sensitivity. Regular Langmuir probes or retarding potential energy analyzers are not suitable since they integrate the particle flux over a wide range of angles in velocity space. Directional curved plate energy analyzers commonly used in space plasma experiments [*Sanderson and Henrion*, 1975] must have dimensions on the order of a Debye length, which is difficult to achieve in dense laboratory plasmas. Recently, we have developed a directional ion energy analyzer based on geometric filtering with microchannel plates [*Stenzel et al.*, 1982*c*]. A similar detector modified for electron velocity analysis is shown schematically in Figure 13.

A metallic microchannel plate containing a multitude of long (1.5 mm), thin (0.2 mm diameter) parallel holes is biased to the local plasma potential. Electrons with velocities within a narrow cone ($\Delta\theta \simeq 8°$, $\Delta\Omega \simeq 1.7 \times 10^{-2}$ sr) can pass through the holes; all others are collected at the channel walls. The energy of the nearly parallel moving particles is analyzed by a plane retarding potential energy analyzer consisting of two grids and a collector. The direction of the velocity analyzer can be varied continuously from parallel to perpendicular to **B** so as to obtain $f(v_{\|}, v_{\perp})$. Except at low energies ($E \lesssim 1$ eV) the perpendicular electron Lamor orbit can still be analyzed due to the small channel dimensions and the low magnetic field strength.

Figure 14 shows electron distribution functions measured at the low potential side (Figure 14*a*) and the high potential side (Figure 14*b*) of the double layer. One can clearly see the evolution of a high-energy tail of electrons accelerated at the double

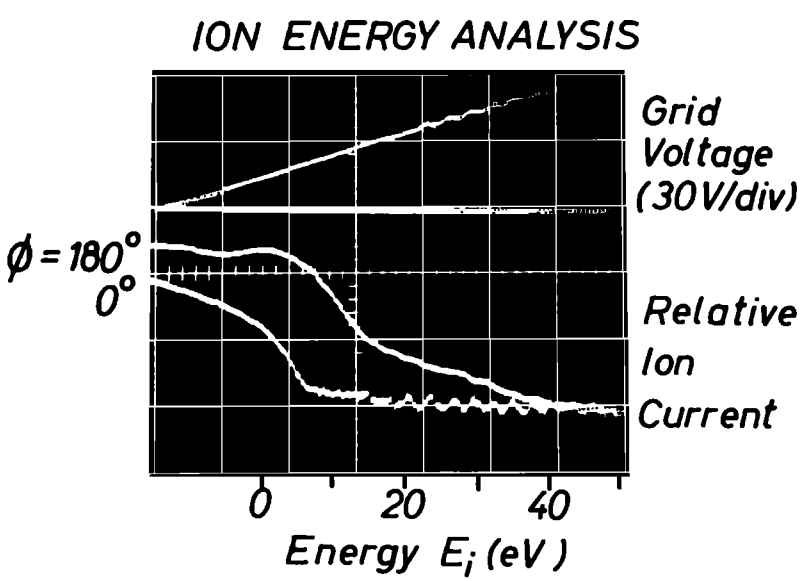

Fig. 15. Ion energy analyzer traces taken at the low-potential side of the double layer ($\Delta y \simeq 8$ cm) during a current disruption ($t \simeq 25$ μs). Top trace: retarding grid potential (0.5 μsec/div). Bottom traces: collector currents with the analyzer pointing toward the double layer ($\phi = 180°$) and away from it ($\phi = 0°$). The large ion flux from the double layer is due to ion acceleration up to $\frac{1}{2}m_i v^2 \simeq e\Delta\phi_p \simeq 35$ eV.

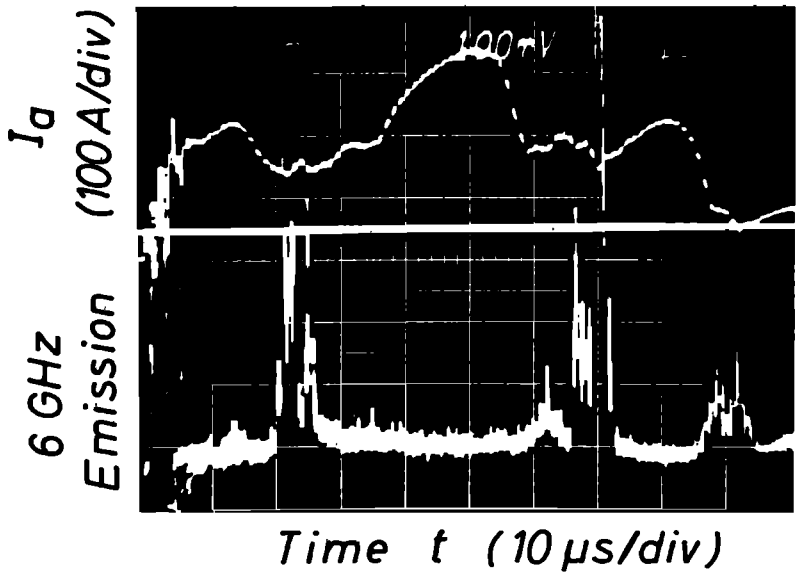

Fig. 16. Dual trace display of the disrupted center plate current $I_{a(t)}$ and the microwave emission observed with an rf probe in the high potential region ($\Delta y \leq 6$ cm). Bursts of electron plasma waves ($\omega \gtrsim \omega_{pe}$) are excited by beam-plasma instabilities associated with the formation of double layers during current disruptions.

layer ($\frac{1}{2}mv^2 \simeq e\Delta\phi_p \simeq 35$ eV). The energetic particles have a beamlike distribution that excites electron plasma waves to be discussed below. The tails also carry most of the plasma current, determine the average kinetic energy, and the energy flow. The fast electrons have acquired their energy from the stored magnetic field energy released during the current disruption.

While electrons at a double layer are accelerated toward the high potential region, ions are energized into the opposite direction. This is confirmed by placing an ion energy analyzer into the low potential region ($\Delta y \simeq 8$ cm) and by observing the ion flux toward and away from the double layer. The current voltage characteristics of Figure 15 indicate that ions streaming away from the double layer ($\phi = 180°$) have energies up to ~ 35 eV corresponding to the potential step. The ion flux in the opposite direction ($\phi = 0°$) is lower and consists of cold ions that will be reflected by the double layer. The large outflow of ions from the high potential region leads to the observed density loss and current drop. The accelerated ions also have gained their energy on expense of the stored magnetic field energy that builds up during the initial plasma current rise. The directed kinetic energy is eventually randomized by collisions and wave-particle interactions.

Microinstabilities

The acceleration of electrons and ions at a double layer forms particle beams whose free energy can drive various instabilities. On the high-potential side, electron plasma waves are excited by the electron beam. These are observed with a movable short wire rf probe connected to a microwave receiver. Figure 16 shows dual traces of the small end plate current $I_{a(t)}$ and the plasma wave emission. At every current disruption a burst of microwave emission is detected. By analyzing the frequency spectrum the emission is found to be near the local electron plasma frequency ($f \gtrsim f_{pe} \simeq 5 \ldots 7$ GHz). A spatial scan shows that the signals are only observed in regions where the accelerated free electrons are present. These features are consistent with the beam-plasma instability studied earlier in this device by electron beam injection [*Whelan and Stenzel*, 1981]. They have also been observed in various other double layer experiments [*Leung et al.*, 1980; *Sato*, 1982; *Lindberg*, 1982; *Hollenstein and Guyot*, 1982].

On the low-potential side of the double layer an enhanced level of low-frequency fluctuations is observed. Streaming ions and drifting electrons provide free energy for instabilities. These involve density fluctuations as pointed out in Figure 10*a* (bottom trace) but also magnetic field fluctuations in a high beta plasma [$\beta = nkT/(B^2/2\mu_0) \approx 1$]. Figure 17 shows magnetic probe signals $\dot{B}_{x(t)}$ at $\Delta y \simeq 30$ cm together with the center end plate current $I_{a(t)}$. In the presence of current disruptions (Figure 17*a*) the fluctuation level is high while at low or zero currents ($I_a = 0$, Figure 17*b*) the magnetic fluctuations are greatly reduced. The frequency spectrum ($f \simeq 0.2 - 1$ MHz) is above the lower hybrid frequency ($\omega_{ce} \cong \omega_{ce}^{1/2}\ \omega_{ci}^{1/2} \simeq 2\pi \times 0.13$ MHz) but well below the electron cyclotron frequency ($\omega_{ce} \simeq 2\pi \times 35$ MHz), i.e., at the low end of the whistler wave branch. Extensive cross-correlation measurements of magnetic turbulence in the current sheet have identified the modes to be oblique whistlers [*Gekelman et al.*, 1983]. Electrostatic low-frequency fluctuations exhibit a dispersion curve of ion acoustic modes [*Stenzel and Gekelman*, 1981*b*]. The exact excitation mechanisms for these instabilities still have to be determined.

DISCUSSION

The different observations of the disruption phenomenon form the basis for a physical model outlined schematically in Figure 18. Triggered by a temporary current drop in the center of the current sheet an inductive voltage LdI_a/dt develops. It increases the plasma potential ϕ_p in the perturbed current channel and generates an inductive electric field $-\dot{A}_y$ both of which would normally restore the current loss. However, when the electron drift velocity approaches the thermal velocity and the density cannot be raised by additional ionization, the current density becomes limited. A double layer forms with a potential drop corresponding approximately to the inductive loop voltage. The electric field accelerates electrons toward the small end plate but ejects ions away from it. The latter causes a net density loss which, in turn, lowers the current density. Thus,

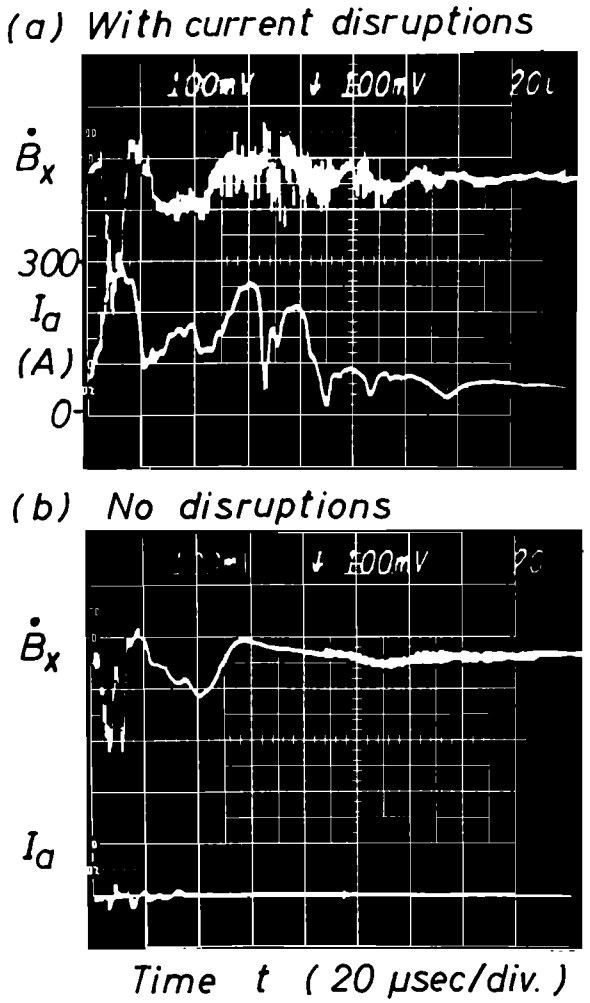

Fig. 17. Magnetic fluctuations associated with current disruptions. (*a*) Magnetic probe signal $\dot{B}_{x(t)}$ at $\Delta y \simeq 30$ cm and center plate current $I_{a(t)}$ with disruptions (*b*) Background magnetic noise at $I_a = 0$.

an unstable feedback loop is established: A current decrease builds up an electric field which further lowers the current. This negative resistance leads to an impulsive current loss. The process is driven by the stored magnetic energy and retarded by ion inertia. The time scale of the current collapse is on the order of an ion transit time through the perturbed current channel ($\Delta t \approx L/\langle v \rangle \approx 6$ cm/6 $\times$ 10^5 cm/s $\simeq$ 10 μs). After the current has reached its minimum the process reverses, i.e., the plasma potential is lowered so as to attract ions that builds up the plasma density and current I_a.

Although the largest particle acceleration is due to the strong electric field of the double layer, there are other electromagnetic forces acting on the particles. An inductive electric field $-\dot{A}_y$ exists generated by the magnetic flux changes inside the plasma. The magnetic force density $\mathbf{j} \times \mathbf{B}$ gives rise to transverse jetting of plasma in an X type magnetic field topology. The loss of current changes the field configuration from a neutral sheet to that of an X point ($\nabla \times \mathbf{B} = 0$). If initially a magnetic island is present the $\mathbf{j} \times \mathbf{B}$ force is stabilizing and no current disruptions are observed.

Thus the observed current disruption with double layer formation in a high beta plasma represents complicated coupled electric and magnetic processes that are three-dimensional and time dependent. Present double layer theories have not yet considered such cases.

It is interesting to speculate whether the presently observed phenomena can occur in related laboratory experiments or in space plasmas. For example, in a neutral point discharge *Ohyabu et al.* [1974] observed a short-duration drop in plasma current and an associated voltage pulse between anode and cathode grids. The external circuit inductance appears essential in explaining the voltage pulse ($\Delta V = L dI/dt$). Electrons and ions with energies corresponding to the voltage pulse are observed but explained by turbulent heating rather than localized potential structures. These are difficult to observe in dense pulsed plasmas but may very well exist.

In space plasmas the observational difficulties of identifying double layers and current systems are even larger than in laboratory plasmas so that comparisons are somewhat speculative. Nevertheless, models of electrical circuits with double layers have been proposed for space plasmas [*Alfvén*, 1977; *Carlqvist*, 1982; *Spicer*, 1982]. *Carlqvist* [1972] describes the evolution of a double layer from a density depression in a current carrying plasma. Although in the present experiment the disruption is near an electrode it could also have developed at other regions where an initial density depression or magnetic field nonuniformity existed. Such conditions are not unlikely to

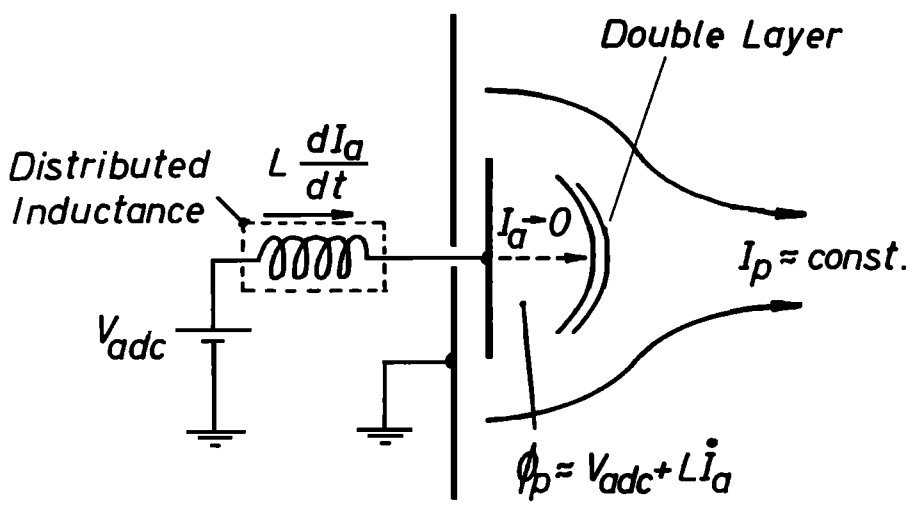

Fig. 18. Schematic diagram of the important elements in the physical model for the disruptive instability (see text).

exist in magnetospheric current systems. Several features of the observed disruptive instability have similarities to substorm phenomena: (1) Current redistribution and release of stored magnetic field energy. (2) Particle energization to levels that cannot be explained by steady-state potentials but involve inductive effects. (3) Localized potential structures and particle acceleration. (4) Excitation of various instabilities drive by the free energy of anisotropic distributions.

Acknowledgments. The authors appreciate assistance in the experiments from J. M. Urrutia and D. A. Whelan. This work was supported by the National Science Foundation grants NSF ATM 81-19717, NSF PHY 82-09524, and by the National Aeronautics and Space Administration under grant NAGW-180.

The Editor thanks S. Torvén and D. S. Spicer for their assistance in evaluating this paper.

REFERENCES

Akasofu, S.-I., *Physics of Magnetospheric Substorms*, D. Reidel, Hingham, Mass., 1977.

Alfvén, H., Electric currents in Cosmic plasmas, *Rev. Geophys. Space Phys.*, *15*(3), 271–284, 1977

Baum, P. J., and A. Bratenahl, Magnetic reconnection experiments, in *Advances in Electrons and Electron Physics*, vol. 54, edited by C. Marton, pp. 1–67, Academic, New York, 1980*a*.

Baum, P. J., and A. Bratenahl, Double layer formation during impulsive flux transfer events, paper presented at Workshop on Space Plasma Physics at the Institute of Geophysics and Planetary Physics, University of California, Los Alamos Scientific Laboratory, Los Alamos, N. Mex., Sept. 4–5, 1980*b*.

Baum, P. J., and A. Bratenahl, The laboratory magnetosphere, *Geophys. Res. Lett.*, *9*(4), 435–438, 1982.

Block, L. P., A double layer review, *Astrophys. Space Sci.*, *55*, 59–83, 1978.

Bulanov, S. V., and S. I. Syrovatskii, Kinetics of a neutral current sheet, *Proc. P. N. Lebedev Phys. Inst. Acad. Sci. USSR Engl. Transl.*, *74*, 87–106, 1976.

Carlqvist, P., On the formation of double layers in plasmas, *Cosmic Electrodyn.*, *3*, 377–388, 1972.

Carlqvist, P., Double layers in space, in *Symposium on Plasma Double Layers*, edited by P. Michelsen and J. J. Rasmussen, Risø-R-472, pp. 255–273, Risø National Laboratory, Roskilde, Denmark, 1982.

Dawson, J. M., Simulation of space plasma phenomena, in *Physics of Auroral Arc Formation, Geophys. Monogr. Ser.*, vol. 25, edited by S.-I. Akasofu and J. R. Kan, pp. 270–282, AGU, Washington, D. C., 1981.

Dreicer, H., Electron and ion runaway in a fully ionized gas, *Phys. Rev.*, *115*, 238–249, 1959.

Dungey, J. W., *Cosmic Electrodynamics*, Cambridge University Press, New York, 1958.

Frank, A. G., Experimental study on the conditions for the appearance of a neutral sheet in a plasma: Some characteristics of the sheet, *Proc. P. N. Lebedev Phys. Inst. Acad Sci. USSR Engl. Transl.*, *74*, 107–163, 1976.

Furth, H. P., J. Killeen, and M. N. Rosenbluth, Finite-resistivity instabilities of a sheet pinch, *Phys. Fluids*, *6*(4), 459–484, 1963.

Gekelman, W., and R. L. Stenzel, Magnetic field line reconnection experiments, 2, Plasma parameters, *J. Geophys. Res.*, *86*, 659–666, 1981.

Gekelman, W., R. L. Stenzel, and N. Wild, Magnetic field line reconnection experiments, 3, Ion acceleration, flows, and anomalous scattering, *J. Geophys. Res.*, *87*, 101–110, 1982.

Gekelman, W., N. Wild, and R. L. Stenzel, Magnetic field line reconnection experiments, 6, Magnetic turbulence, *J. Geophys. Res.*, *88*, in press, 1983.

Hayashi, T., and T. Sato, Magnetic reconnection: Acceleration, heating, and shock formation, *J. Geophys. Res.*, *83*, 217–220, 1978.

Heikkila, W. J., and R. J. Pellinen, Localized induced electric fields within the magnetotail, *J. Geophys. Res.*, *82*, 1610–1614, 1977.

Hollenstein, C. and M. Guyot, Experiments on potential gradients in a current carrying plasma, Part II, Turbulence, *Rep. LRP 210/82*, Ecole Polytechnique Fédérale de Lausanne, Switzerland, June 1982.

Iizuka, S., P. Michelsen, J. J. Rasmussen, R. Schrittwieser, R. Hatakeyama, K. Saeki, and N. Sato, Dynamics of a potential barrier formed on the tail of a moving double layer in a collisionless plasma, *Phys. Rev. Lett.*, *48*(3), 145–148, 1982.

Langmuir, I., The interaction of electron and positive ion space charges in cathode sheaths, *Phys. Rev.*, *33*, 954, 1929.

Leboeuf, J. N., T. Tajima, and J. M. Dawson, Dynamic magnetic X points, *Phys. Fluids.*, *25*(5), 784–799, 1982.

Leung, P., A. Y. Wong, and B. H. Quon, Formation of double layers, *Phys. Fluids*, *23*(5), 992–1004, 1980.

Lindberg, L., Experimental studies of electron scattering due to beam-plasma interaction near a double layer, in *Symposium on Plasma Double Layers*, edited by P. Michelsen and J. J. Rasmussen, Risø-R-472, pp. 164–169, Risø National Laboratory, Roskilde, Denmark, 1982.

McPherron, R. L., Magnetospheric substorms, *Rev. Geophys. Space Phys.*, *17*, 657–681, 1979.

Ohyabu, N., S. Okamura, and N. Kawashima, Simulation experiment of the current dissipation and plasma acceleration in the neutral sheet, *J. Geophys. Res.*, *79*, 1977–1979, 1974.

Podgorny, I. M., E. M. Dubinin, and Y. N. Potanin, On magnetic curl in front of the magnetosphere boundary, *Geophys. Res. Lett.*, *7*, 247, 1980.

Potemra, T. A., Current systems in the earth's magnetosphere, *Rev. Geophys. Space Phys.*, *17*, 640–656, 1979.

Quon, B. H., and A. Y. Wong, Formation of potential double layers in plasmas, *Phys. Rev. Lett.*, *31*, 1393–1396, 1976.

Roederer, J. G., Earth's magnetosphere: Global problems in magnetospheric physics, in *Space Plasma Physics: The Study of Solar Systems Plasmas*, vol. 1, part II, pp. 373–451, National Academy of Sciences, Washington, D. C., 1979.

Sanderson, T. R., and J. Henrion, Measurement of the geometrical factor of an electrostatic analyzer-channeltron detector, *Space Sci. Instrum.*, *1*, 351–361, 1975.

Sato, N., Double layers in laboratory plasmas, in *Symposium on Plasma Double Layers*, edited by P. Michelsen and J. J. Rasmussen, Risø-R-472, pp. 116–140, Risø National Laboratory, Roskilde, Denmark, 1982.

Sato, T., and H. Okuda, Numerical simulation of ion acoustic double layers, *J. Geophys. Res.*, *86*, 3357–3368, 1981.

Schamel, H., The theory of double layers, in *Symposium on Plasma Double Layers*, edited by P. Michelsen and J. J. Rasmussen, Risø-R-472, pp. 13–39, Risø National Laboratory, Roskilde, Denmark, 1982.

Smith, R. A., Vlasov simulation of plasma double layers, *Physica Scripta*, *25*, 413–415, 1982.

Spicer, D. S., Magnetic energy storage and conversion in the solar atmosphere, *Space Sci. Rev.*, *31*, 351–435, 1982.

Stenzel, R. L., and W. Gekelman, Magnetic field line reconnection experiments, 1, Field topologies, *J. Geophys. Res.*, *86*, 649–658, 1981*a*.

Stenzel, R. L., and W. Gekelman, Laboratory experiments on magnetic field line reconnection, paper presented at the XV International Conference on Phenomena in Ionized Gases, Minsk, USSR, July 14–18, 1981*b*.

Stenzel, R. L., M. Ooyama, and Y. Nakamura, Potential double layers in strongly magnetized plasmas, in *Physics of Auroral Arc Formation, Geophys. Monogr. Ser.*, vol. 25, edited by S.-I. Akasofu and J. R. Kan, pp. 226–233, AGU, Washington, D. C., 1981.

Stenzel, R. L., W. Gekelman, and N. Wild, Double layer formation during current sheet disruptions in a reconnection experiment, *Geophys. Res. Lett.*, *9*, 680–683, 1982*a*.

Stenzel, R. L., W. Gekelman, and N. Wild, Magnetic field line reconnection experiments, 4, Resistivity, heating, and energy flow, *J. Geophys. Res.*, *87*, 111–117, 1982*b*.

Stenzel, R. L., R. Williams, R. Agüero, K. Kitazaki, A. Ling, T. McDonald, and J. Spitzer, A novel directional ion energy analyzer, *Rev. Sci. Instrum.*, *53*(7), 1027–1031, 1982*c*.

Stenzel, R. L., W. Gekelman, and N. Wild, Electron distribution functions in a current sheet, *Phys. Fluids*, in press, 1983.

Stern, D. P., Large scale electric fields in the earth's magnetosphere, *Rev. Geophys. Space Phys.*, *15*, 156–194, 1977.

Syrovatskii, S. I., Pinch sheets and reconnection in astrophysics, *Ann. Rev. Astron. Astrophys.*, *19*, 163–229, 1981.

Torvén, S., Formation of double layers in laboratory plasmas, in *Wave Instabilities in Space Plasmas*, edited by P. J. Palmadesso and K. Papadopolous, pp. 109–128, D. Reidel, Hingham, Mass., 1979.

Torvén, S., and M. Babić, Current chopping space charge layers in a

low pressure arc plasma, *Proceedings 12th International Conference on Phenomena in Ionized Gases*, part I, p. 124, Elsevier, New York, 1975.
Tuma, D. T., and A. A. Ware, Magnetically induced current chopping in low pressure discharges, *Phys. Fluids*, *11*(6), 1206–1215, 1968.
Whelan, D. A., and R. A. Stenzel, Electromagnetic wave excitation in a large laboratory beam-plasma system, *Phys. Rev. Lett.*, *47*, 95–98, 1981.

(Received January 11, 1983;
revised March 11, 1983;
accepted March 14, 1983.)